NANO LETTERS

pubs.acs.org/NanoLett Letter

Engineering Interlayer Electron−Phonon Coupling in WS_2/BN Heterostructures

Yifei Li,[ⓘ] Xiaowei Zhang,[ⓘ] Jinhuan Wang, Xiaoli Ma, Jin-An Shi, Xiangdong Guo, Yonggang Zuo, Ruijie Li, Hao Hong, Ning Li, Kai Xu, Xinyu Huang, Huifeng Tian, Ying Yang, Zhixin Yao, PeiChi Liao, Xiao Li, Junjie Guo, Yuang Huang, Peng Gao, Lifen Wang, Xiaoxia Yang, Qing Dai, EnGe Wang, Kaihui Liu, Wu Zhou, Xiaohui Yu, Liangbo Liang, Ying Jiang, Xin-Zheng Li,* and Lei Liu*

Cite This: *Nano Lett.* 2022, 22, 2725−2733 Read Online

ACCESS | Metrics & More | Article Recommendations | Supporting Information

ABSTRACT: In van der Waals (vdW) heterostructures, the interlayer electron−phonon coupling (EPC) provides one unique channel to nonlocally engineer these elementary particles. However, limited by the stringent occurrence conditions, the efficient engineering of interlayer EPC remains elusive. Here we report a multitier engineering of interlayer EPC in WS_2/boron nitride (BN) heterostructures, including isotope enrichments of BN substrates, temperature, and high-pressure tuning. The hyperfine isotope dependence of Raman intensities was unambiguously revealed. In combination with theoretical calculations, we anticipate that WS_2/BN supercells could induce Brillouin-zone-folded phonons that contribute to the interlayer coupling, leading to a complex nature of broad Raman peaks. We further demonstrate the significance of a previously unexplored parameter, the interlayer spacing. By varying the temperature and high pressure, we effectively manipulated the strengths of EPC with on/off capabilities, indicating critical thresholds of the layer−layer spacing for activating and strengthening interlayer EPC. Our findings provide new opportunities to engineer vdW heterostructures with controlled interlayer coupling.

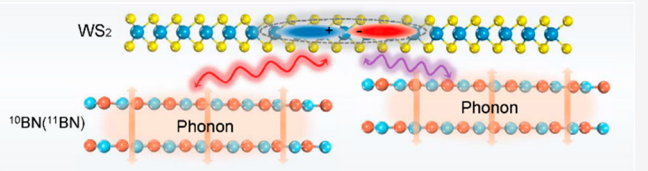

KEYWORDS: *vdW heterostructure, isotope engineering, high-pressure engineering, electron−phonon coupling, interlayer spacing*

INTRODUCTION

van der Waals (vdW) heterostructures assembled from two-dimensional (2D) crystals serve as a powerful platform for exploring exotic properties and novel quantum phenomena.[1,2] Particles/quasiparticles, including electrons and phonons spatially residing in different layers, can be tightly bound by interlayer interactions, resulting in several fascinating phenomena and potentials for electronic and optoelectronic devices.[3−6] For instance, electron−hole pairs in adjacent transition-metal dichalcogenide (TMD) layers can bind into interlayer excitons.[4] In transferred TMD/boron nitride (BN) vdW heterostructures, phonons in BN couple to electronic transitions of TMDs when the incident photons resonate with certain excitons in TMDs, activating optically silent phonon modes of BN in Raman scattering.[5,6] In TMDs/amorphous SiO_2 heterostructures, interlayer electron−phonon coupling (EPC) activated phonons of SiO_2 can participate in exciton intervalley scatterings.[7,8] Conventionally, studies of EPC have been focused on one material for a variety of physical phenomens, including carrier scattering, conventional superconductivity, Kohn anomalies, and optical properties.[9] Very recently, interlayer EPC across the vdW gap in layered-crystal heterostructures[5−8,10,11] has emerged as a new territory which provides a unique opportunity to manipulate electrons and phonons nonlocally.

In an effort to uncover the mechanism of interlayer EPC, Chow et al. have proposed one microscopic, phenomenological approach where an out-of-plane phonon mode in TMDs is critical and bridges the coupling between BN phonons and TMD excitons.[8] In TMD layers, this particular phonon interacts with excitons by an intralayer EPC, and two out-of-plane phonons separated by a vdW gap (one in TMD layers and the other in BN layers) can be coupled together by an interlayer dipole−dipole interaction. With regard to its manipulation, electrostatic doping that works for conventional EPC tuning in one material has been demonstrated for interlayer EPC with poor efficiency, yielding completely disappearing Raman signals at a relatively low doping level.[5,11] A postannealing treatment enhanced the coupling strength at interfaces of TMDs and SiO_2.[7] Despite these

Received: November 30, 2021
Revised: March 11, 2022
Published: March 16, 2022

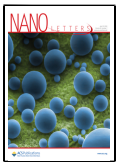

https://doi.org/10.1021/acs.nanolett.1c04598
Nano Lett. 2022, 22, 2725−2733

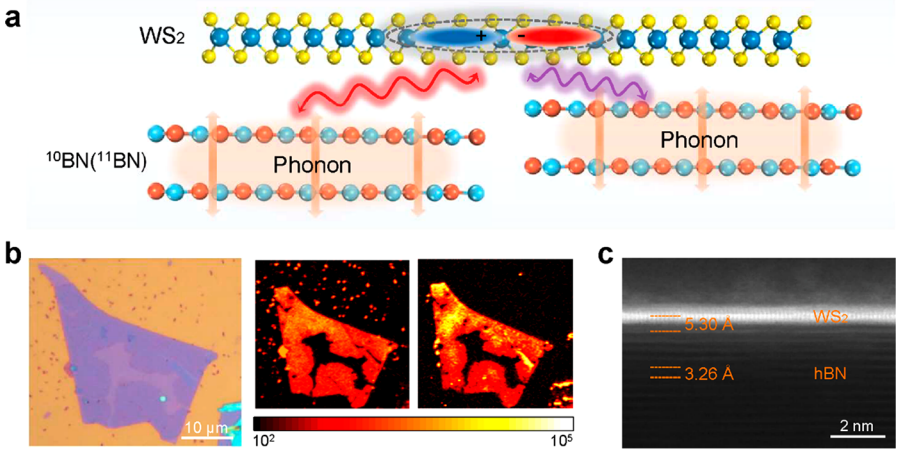

Figure 1. Engineering interlayer EPC in vdW heterostructure of WS_2 and BN. (a) Illustration of multitier engineering means of interlayer electron (in WS_2) and phonon (in BN) coupling, including isotope engineering in BN, temperature, and pressure. (b) Representative optical image (left panel) of one vdW heterostructure, showing partially covered WS_2 islands by CVD. Raman (middle panel) and PL mapping (right panel) were conducted to confirm the quality and targeted areas with good uniformity for further measurements. (c) Cross-sectional STEM image, showing the contamination-free interface and close contact between WS_2 and BN.

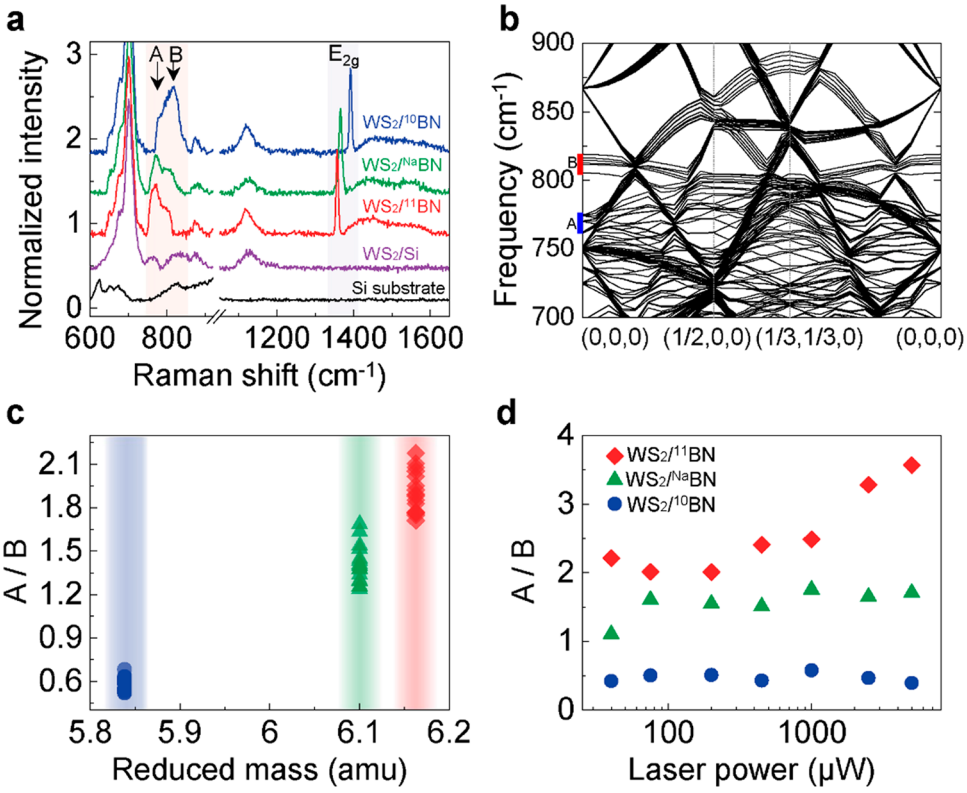

Figure 2. Isotopically dependent Raman spectra. (a) Raman spectra of WS_2 and vdW heterostructures with 2.33 eV excitation, on resonance with the B exciton in WS_2, showing in the heterostructures the presence of two asymmetrical and broad peaks around 800 cm^{-1} assigned to A and B modes in BN. (b) Calculated phonon dispersion of ML-WS_2/six-layer-^{Na}BN heterostructure. The blue (red) rectangle represents the theoretical assignment for the A (B) mode. (c) Statistics of the intensity ratio of A and B peaks (A/B) from more than 50 heterostructures, showing distinct isotope dependence. (d) Intensity ratio A/B as a function of the laser power in the range of 40 μW and 5 mW, displaying a constant value of ~0.5 in $WS_2/^{10}$BN stacks and a fluctuating ratio from 2.0 to 3.5 in $WS_2/^{11}$BN heterostructures.

advances, an in-depth understanding and efficient engineering of interlayer EPC remain in their infancy. Therefore, a multitier approach utilizing a series of experimental techniques to tackle this problem is highly desirable. This not only can expand practical potentials of interlayer EPC but also provide a glimpse into its underlying mechanism.

Here we report the isotope, temperature, and high-pressure engineering of interlayer EPC, as illustrated in Figure 1a, in directly grown and conventionally transferred WS_2/BN heterostructures. The phonon engineering by isotopic substitutions of BN layers reveals unprecedented isotope-dependent Raman intensities, suggesting the WS_2/BN supercell-induced complexity of phonon structures in the process of

https://doi.org/10.1021/acs.nanolett.1c04598
Nano Lett. 2022, 22, 2725−2733

interlayer coupling. Our study demonstrates the significance of the interlayer spacing between TMDs and BN layers. By tuning the interfacial spacing through temperature and pressure, we can effectively manipulate the strength of the interlayer coupling with the capabilities of turn-on and -off.

RESULTS

Isotopically Engineered WS_2/BN Heterostructures. First we examined the isotope disorder effect on interlayer EPC by purifying BN substrates as ^{10}BN or ^{11}BN. By a molten metal flux method, isotopically enriched BN crystals were synthesized at high temperature (~1600 °C, Methods and Materials and Figure S1 in the Supporting Information) using boron powder with an ultrahigh isotope purity.[12] In comparison with the natural isotope variation (20.1 atom % ^{10}B and 79.1 atom % ^{11}B), boron-10 (97.18 atom % ^{10}B) and boron-11 (99.69 atom % ^{11}B) powders and ultrahigh-purity N_2 (naturally 99.6 atom % ^{14}N) ensure the monoisotopic characteristic of as-grown BN crystals.[13,14] We performed Raman, Fourier-transform infrared (FTIR), and vibrational electron energy loss spectroscopy (EELS) measurements, confirming the atomic-mass-dependent frequency of lattice vibrations that is one natural consequence of isotope engineering[15−17] (Figure S1). Next, isotopically engineered heterostructures were prepared by the chemical vapor deposition (CVD) of WS_2 on tape-exfoliated BN flakes[18] (Methods and Materials).

Instead of mechanical stacking where impurities at the interface are inevitable, the growth of WS_2 on prefabricated BN flakes provides polymer-free interfaces, large-scale uniformity, and more importantly, a close contact between WS_2 and BN by the high growth temperature (>900 °C). Heterostructures with a BN thickness of 20−100 nm were deliberately chosen. Figure 1b displays an optical image of one representative heterostructure, clearly showing partially covered WS_2 domains. 2D Raman and photoluminescence (PL) mappings show wrinkles and grain boundaries, consistent with features observed from optical images. The area with uniform optical properties (~3 μm by 3 μm) was selected for further investigations. The high-quality interface is directly confirmed at the atomic level by the cross-section image of a scanning transmission electron microscope (STEM). Figure 1c displays one representative BN flake−WS_2 monolayer (ML) interface, clearly showing the contaminant-free vdW interface. While the layer distance in BN flakes is 3.26 Å, the interlayer spacing between the BN and W layers is 5.30 Å, and the BN−sulfur layer−layer distance is ~3.2 Å, demonstrating eliminated differences in layer spacing in CVD-grown heterostructures.

Isotopically Dependent Raman Spectra. Raman measurements on three types of heterostructures were performed at room temperature (RT) with an excitation energy of 2.33 eV, which resonates with the B exciton of WS_2.[10] Figure 2a shows the typical results from heterostructures and the standalone CVD-grown WS_2 on the substrate (Figure S2a and Table S1). The most notable observation is the presence of several peaks that cannot be assigned to Raman-active modes from the SiO_2/Si substrate, WS_2, or BN, including two broad peaks within 1400−1600 cm^{-1} and peaks at around 800 cm^{-1}. As exemplified by the WS_2/natural BN (^{Na}BN) heterostructure, two emerging Raman peaks are located at 772 and 805 cm^{-1}, respectively (Figure S2c), which were previously attributed to the interlayer EPC-induced BN A_{2u} mode of the ZO_2 branch and the B_{1g} mode in the ZO_3 branch, respectively.[10] From the aspect of symmetry, while the envelope of the B exciton wave function is azimuthally symmetrical with the orbitals pointing along the z direction, A_{2u} and B_{1g} modes in BN involve out-of-plane vibrations along z (Figure S3a).[19] The intensity of interlayer EPC-induced Raman peaks can be tremendously enhanced when the irradiated laser resonates with one specific exciton of TMDs.[5,6,8] The combination of WS_2 and 2.33 eV power of the laser was chosen deliberately in our experiment.[10] Also, the strong EPC detected in our heterostructures corroborates the high quality of crystals and interface by the CVD growth.

We found that these two peaks possess highly asymmetrical line shapes and are much broader than E_{2g} Raman peaks: the full widths at half-maximum (fwhm) of 24 and 45 cm^{-1} for the two peaks are in marked contrast to 7.5 cm^{-1} for the E_{2g} mode of BN. Theoretical investigations for phonon band structures were performed, and the calculated phonon dispersion of ML-WS_2/six-layer-^{Na}BN heterostructure is shown in Figure 2b (Note 1 and Figure S3 in the Supporting Information). Due to the lattice mismatch, a supercell between BN and WS_2 in the heterostructures means that the ZO phonon branches of BN are folded, leading to two groups of phonon modes labeled by A and B in Figure 2b. Superpositions of these modes are believed to be responsible for two broad peaks at around 800 cm^{-1} in Raman spectra. So far, all of the experimentally observed Raman peaks induced by interlayer EPC possess much larger fwhms (including phonon modes of SiO_2), supporting our explanation (Note 1 in the Supporting Information). Here we emphasize that the supercell of BN and TMDs renders BN phonons involved in interlayer EPC much more complicated. This supercell-induced complex nature of BN phonons not only blurs the precise recognition of exact atomic vibration modes that couple to electrons but also obscures the microscopic mechanism of interlayer EPC that we will show later.

Interestingly, an apparent isotope effect on A and B peaks was also observed. EPC-induced peaks exhibit a significant frequency shift upon isotopic boron substitutions: 787 cm^{-1} (A) and 817 cm^{-1} (B) in ^{10}BN stacks, in comparison with 767 cm^{-1} (A) and 800 cm^{-1} (B) in ^{11}BN heterostructures (Figure S2b−d), demonstrating the frequency dependence on atomic mass for induced but originally silent Raman peaks.[20,21] Moreover, in Figure 2a we found that the B peak is higher than the A peak for the WS_2/^{10}BN sample, while the A peak is more predominant in the WS_2/^{11}BN heterostructure (Figure S2). We then carried out Raman measurements on multiple heterostructures (more than 50) and summarize the intensity ratio of A and B peaks (A/B) in Figure 2c, unambiguously showing the same behavior in all samples, despite the variation of BN thickness. Additionally, the results of excitation-power-dependent Raman measurements (Figure S4a) are summarized in Figure 2d. In ^{10}BN systems A/B is consistently about 0.5; for WS_2/^{11}BN samples A/B increases from ~2.0 to 3.5 with the laser power. By variation of the excitation power, the density of the B exciton in WS_2 is consequently modulated. It turns out that the isotope dependence of Raman intensities is insensitive to the laser power or exciton density, indicating that it could be an intrinsic characteristic affiliated with isotopically engineered vdW heterostructures. Furthermore, this isotope-governed Raman spectrum is quite robust, and the same phenomena can be observed after 1 year of sample storage in air (Figure S4b).

https://doi.org/10.1021/acs.nanolett.1c04598
Nano Lett. 2022, 22, 2725−2733

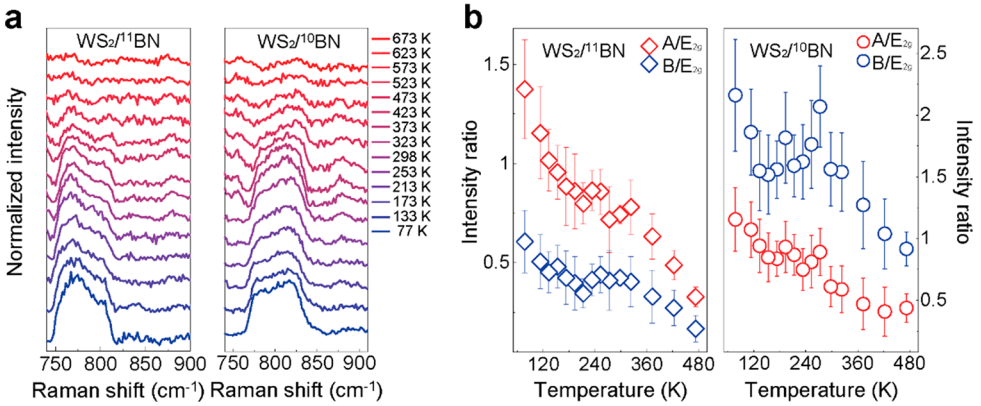

Figure 3. Temperature-dependent measurements. (a) Raman spectra of $WS_2/^{11}BN$ (left panel) and $WS_2/^{10}BN$ (right panel) heterostructures from 77 to 673 K. The interlayer EPC-induced Raman peaks were enhanced at low temperature and gradually vanished above 476 K for both heterostructures. (b) Intensity ratios between the A (B) and E_{2g} peaks in two types of heterostructures as a function of temperature, showing the same monotonic response.

The previous experiment showed that atomic displacement parameters are larger for ^{10}BN than for ^{11}BN crystals, constitutionally leading to different dipole strengths (Figure S5).[13] One possible interpretation for isotope-sensitive Raman intensities could be that by the isotope substitution in BN, interlayer dipole−dipole interactions can be consequently modulated, engineering interlayer EPC.[8] For bulk BN, the A_{2u} and B_{1g} modes have the same intralayer vibrational pattern but the opposite interlayer vibrational pattern: i.e., antiphase displacement in adjacent layers for the A_{2u} mode while in-phase in adjacent layers for the B_{1g} mode (Figure S5). As a result, the A_{2u} mode possesses an out-of-plane interlayer electric dipole, while the B_{1g} mode does not.[10] Because the interlayer electric dipole is proportional to the atomic displacement amplitudes, we expect that the interlayer dipole of the A_{2u} mode could be larger for ^{10}BN than for ^{11}BN, which might give rise to the larger interlayer dipole−dipole interaction and stronger A peak Raman intensity in ^{10}BN systems than in ^{11}BN systems. However, this analysis is inconsistent with our experimental observation of A/B in Figure 2a. As was discussed above, phonon branches of BN are folded due to WS_2/BN supercells in the heterostructures; therefore, both A and B peaks actually correspond to mixtures of multiple phonon modes. This significantly complicates the situation, which probably renders the simple model based on the dipole−dipole interactions of A_{2u} and B_{1g} modes invalid to explain our experimental findings. Namely, instead of vibration modes in freestanding BN, we need to consider the "renormalized" BN phonons by TMD/BN supercells at the interface. Direct theoretical calculations of interlayer EPC in isotopically engineered heterostructures are required for a full understanding; however, such calculations are computationally prohibitive due to large supercell sizes and atom number. In addition, theoretical estimations of interlayer EPC were performed by investigating the band gap renormalizations caused by A and B branches (Note 2 in the Supporting Information), in which the interlayer EPC was further confirmed but its isotope dependence still could not be well understood.

Isotopically dependent Raman spectra of vdW heterostructures clearly revealed one characteristic of interlayer EPC: that is, the supercell-induced complexities in both the phonon structures and the consequent interlayer dipole−dipole interactions. Moreover, in our experiment isotope effects on 2D crystals have extended to isotope vdW heterostructures.[13,14,22,23]

Temperature Tuning. As displayed in Figure 3a, in the range of 77−473 K the intensities of EPC-induced A and B peaks decrease unambiguously with increased temperature and signals vanish above 476 K for both ^{10}BN and ^{11}BN systems. Two prominent vibrational modes, E^1_{2g} and A_{1g}, of WS_2 can be obviously observed within the same temperature range, indicating the unaltered sample quality (Figure S4c). In sharp contrast, originally Raman active shear and breathing modes of BN flakes are quite robust at high temperatures.[15−17,24] We further checked the $WS_2/^{Na}BN$ heterostructures, verifying the same temperature-dependent behaviors (Figure S4d). Furthermore, Raman spectra reappeared when the temperature was returned to RT and exhibited the same modulation when the temperature was varied again, demonstrating a controlled, reversible, and nondestructive response. To deduce the conventional temperature effect of phonons, the intensity ratio between the A (B) peak and the E_{2g} mode is summarized in Figure 3b, showing the monotonic decrease upon an increase in temperature and the isotope dependence of A/B.

This discrepancy demonstrates that the temperature can be utilized to tune EPC-induced Raman intensities, probably by modulating the strength of interlayer EPC. We first consider the energy resonance prerequisite for interlayer EPC, since excitons of ML WS_2 shift to higher energy with decreasing temperature. The synchronously acquired temperature-dependent PL spectra present an apparent blue shift of ∼0.17 eV for the A exciton from 673 to 77 K (Figure S4e). With regard to the B exciton of ML WS_2, previous studies show that its energy shifts from 2.37 eV at RT to 2.44 eV at 100 K,[25] indicating an increased mismatch between photon and exciton energies when the temperature is reduced. This larger deviation from the energy resonance at lower temperature contradicts the observed enhanced EPC at a cryogenic temperature. In addition, when the energy resonance meets at RT, temperature alteration toward either side (up or down) will aggravate the divergence, leading to the Λ-shaped EPC strength opposite to the observed monotonic behavior. Second, while the more efficient excitonic effect at low temperatures can be utilized to interpret the enhanced A and B peaks, it can be quite challenging to explain the complete absence of EPC Raman signals at elevated temperatures along

https://doi.org/10.1021/acs.nanolett.1c04598
Nano Lett. 2022, 22, 2725−2733

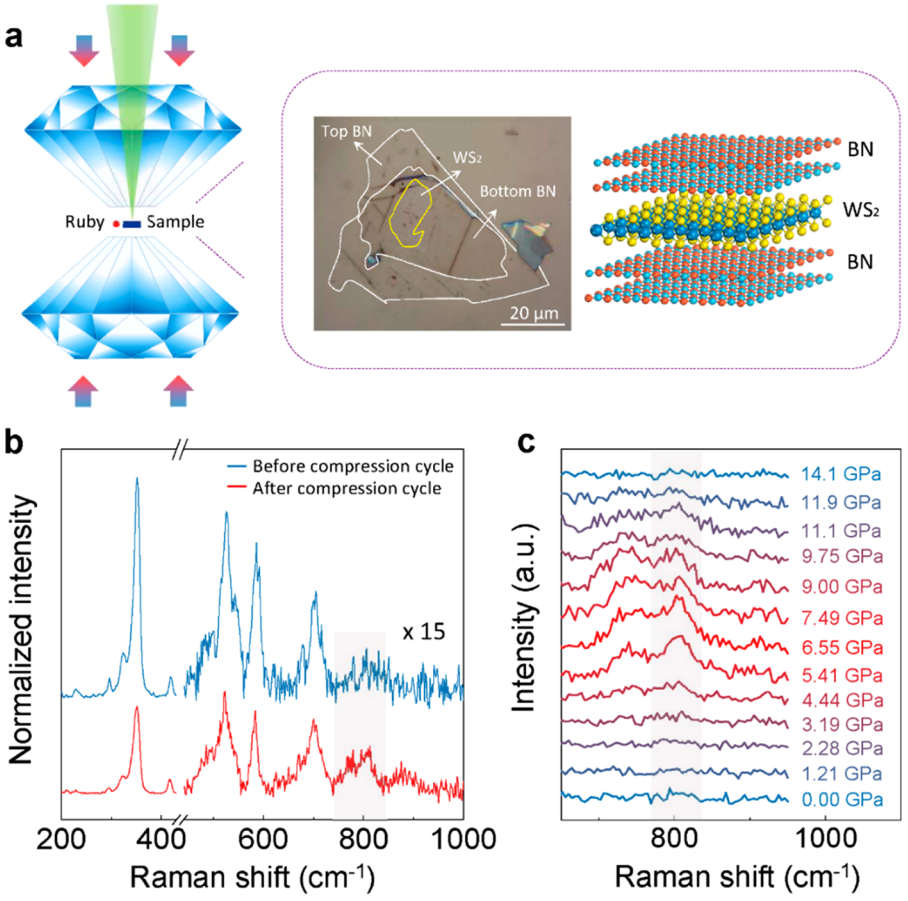

Figure 4. Pressure engineering in transferred WS_2/BN heterostructures. (a) Left panel: schematic of BN-sandwiched WS_2 in a DAC for high-pressure experiments. Right panel: optical micrograph of the BN/WS_2/BN heterostructure on the diamond substrate. (b) Raman spectra of BN/WS_2/BN heterostructure taken before (blue line) and after the compression cycle (red line). The EPC signal (gray rectangle) is obviously enhanced with the other Raman peaks of WS_2 remaining unchanged. (c) Raman spectra of the EPC-induced Raman modes (gray rectangle) in the BN/WS_2/BN heterostructure under different pressures, showing an "off−on−off" response with respect to pressure.

this direction, as the A exciton emission survives at high temperatures (Figure S4e).

Another significant parameter determining the coupling strength is the physical layer−layer spacing between BN and WS_2, which is strongly and positively related to temperature.[26] As a result of the weak vdW bonding, large tuning in layer spacing by thermal expansion has been revealed in vertically stacked heterostructures and drove a direct−indirect band gap transition for a MoS_2−WS_2 bilayer.[27,28] Here, the interlayer spacing increases with increasing temperature, and thus the interlayer EPC is weakened, contributing to the decrease in Raman intensities. In other words, the interlayer coupling of phonons and electrons can be largely engineered by thermally tuning the layer−layer distance. In comparison with engineering a conventional EPC in one material, for example, electrostatic gating to change the electron screen, for interlayer EPC with a nonlocal feature (coupling across the vdW gap), a precise tuning by the electron/exciton density (Figure 2d) failed. Instead, interlayer EPC responds significantly to the physical distance in a controlled, reversible, and nondestructive way, which even can turn "on and off" the coupling at low and high temperatures, respectively. Furthermore, the threshold for activating interlayer EPC is ∼3.20−3.23 Å by an estimation with the thermal expansion of WS_2 and BN crystals (Note 3 and Figure S7 in the Supporting Information).[29]

High-Pressure Experiments. Pressure engineering has been further performed for a better understanding of the mechanism of interlayer EPC. We applied hydrostatic pressure using a diamond anvil cell (DAC), a powerful tool capable of tuning the vibrational and electronic properties of materials (Figure 4a).[30−33] To minimize the influence of diamond substrates, vdW heterostructures of ML WS_2 encapsulated in BN flakes (thickness 5−20 nm) were constructed by a vdW pick-up and then transferred onto the DAC.[34] In contrast to CVD-grown vdW heterostructures, these stacks by transfer show a faint Raman signal at around 800 cm^{-1}, signifying the relatively poor contact between WS_2 and BN layers and consequent weak interlayer coupling solely by transfer (Figure 4b). Surprisingly, after one load−unload cycle of high pressure, two legible Raman peaks located at 774 and 805 cm^{-1} can be observed with uninfluenced Raman peaks of WS_2 between 300 and 750 cm^{-1}, strongly suggesting an irreversible improvement of a WS_2/BN contact and interface quality. By compression of the WS_2/BN spacing, the high pressure strengthens the layer−layer coupling in systems with originally poor interlayer interactions.

Raman measurements at various pressures were conducted to probe the transition and any intermediate states. For two prominent vibrational modes (E^1_{2g} and A_{1g}) of WS_2 (Figure S8a), one can see the hardening of both modes with pressure (Figure S8b), consistent with previous studies.[35−37] We

https://doi.org/10.1021/acs.nanolett.1c04598
Nano Lett. 2022, 22, 2725−2733

noticed the gradual disappearance of the two peaks at a pressure higher than 10.8 GPa, which is induced by high lattice distortions. As shown in Figure 4c, EPC signals are absent below 3.2 GPa and gradually increase with pressure (up to 9 GPa) and eventually disappear on application of a pressure above 11.9 GPa. We correlate this finding with the pressure-compressed interlayer spacing. The absence of EPC-induced Raman peaks verifies the poor layer−layer contact by the mechanical transfer in an ambient environment, in contrast to CVD-grown samples. With increasing pressure, the interlayer spacing can be largely reduced[35,37] and reaches the threshold distance for effective interlayer coupling. The interlayer spacing under 9 GPa is further estimated to be ∼2.75−2.99 Å (Note 4 in the Supporting Information). The disappearance of EPC signals at higher pressure is then attributed to a large lattice distortion, consistent with the Raman behaviors (Figure S8a). Measurements on more WS_2/BN heterostructure exhibit the same pressure dependence (Figure S8c).

It has been shown that the electronic structures of monolayer TMDs and its heterostructures can be well tuned by high pressure.[33] For example, our synchronized PL measurements on ML WS_2 also reveal a clear blue shift at 1.95 GPa and signal quenching occurring at ∼3.83 GPa, indicating a pressure-induced direct−indirect band gap transition (Figure S8d). Our Raman results show that, in addition to the interlayer electron−hole interaction, interlayer coupling between phonons and electrons can be enhanced as well through reduced physical layer−layer distances when high pressure is applied in vdW heterostructures. By combining the findings of temperature and pressure tunings, we conclude that there could be one critical threshold of the BN−WS_2 interlayer spacing to determine whether the interlayer coupling occurs or not.

DISCUSSION

The emerging interlayer EPC is one advantage for vdW heterostructures as one nonlocal way of modulating the electron and phonon behaviors across vdW gaps. While the underlying mechanism is not well understood, in terms of engineering previously only electrostatic doping and post-annealing have been demonstrated, and both unfortunately did not shed more light on the fundamental mechanism. In the present work, by tuning the isotope disorder degree on the "phonon" side, we revealed the robust and hyperfine fingerprint of isotope dependence that emphasizes the intrinsic complexity of interlayer EPC originating from the BN−WS_2 supercell. The temperature tuning deciphers the existence of an interlayer threshold for initiating the effective interfacial coupling; high pressure enhances the coupling of electrons and phonons in systems with poor contacts. Temperature and pressure engineering both emphasize one critical but previously less explored parameter, the physical interlayer distance. The computationally demanding calculations of EPC coupling strength in WS_2/BN heterostructures as a function of interlayer spacing would be highly beneficial to gain a fundamental understanding of the effects of isotope, temperature, and pressure on interlayer EPC-activated Raman events. Our work on engineering interlayer EPC not only advances the understanding of nonlocal particles/quasiparticles interactions but also enables practical ways to engineer vdW heterostructures with potentials for novel electronic and optoelectronic applications.[5,38]

ASSOCIATED CONTENT

Supporting Information

The following files are available free of charge. The Figures S1−S8; Table S1 (PDF) The Supporting Information is available free of charge at https://pubs.acs.org/doi/10.1021/acs.nanolett.1c04598.

Assignments of emergent Raman peaks induced by EPC, theoretical estimate of interlayer EPC, estimation of temperature-dependent BN-WS_2 interlayer spacings, estimation of the pressure dependence of BN−WS_2 interlayer spacings, materials and methods, and additional figures and a table as described in the text (PDF)

AUTHOR INFORMATION

Corresponding Authors

Lei Liu − *School of Materials Science and Engineering, Peking University, Beijing 100871, People's Republic of China; Interdisciplinary Institute of Light-Element Quantum Materials and Research Center for Light-Element Advanced Materials, Peking University, Beijing 100871, People's Republic of China;* orcid.org/0000-0002-7226-8423; Email: l_liu@pku.edu.cn

Xin-Zheng Li − *State Key Laboratory for Artificial Microstructure and Mesoscopic Physics, Frontiers Science Center for Nano-optoelectronics, School of Physics and Interdisciplinary Institute of Light-Element Quantum Materials and Research Center for Light-Element Advanced Materials, Peking University, Beijing 100871, People's Republic of China;* orcid.org/0000-0003-0316-4257; Email: xzli@pku.edu.cn

Authors

Yifei Li − *School of Materials Science and Engineering, Peking University, Beijing 100871, People's Republic of China*

Xiaowei Zhang − *International Center for Quantum Materials, School of Physics and State Key Laboratory for Artificial Microstructure and Mesoscopic Physics, Frontiers Science Center for Nano-optoelectronics, School of Physics, Peking University, Beijing 100871, People's Republic of China*

Jinhuan Wang − *State Key Lab for Mesoscopic Physics and Frontiers Science Center for Nano-optoelectronics, Collaborative Innovation Center of Quantum Matter, School of Physics, Peking University, Beijing 100871, People's Republic of China;* orcid.org/0000-0001-5569-8520

Xiaoli Ma − *Beijing National Laboratory for Condensed Matter Physics, Institute of Physics, Chinese Academy of Sciences, Beijing 100190, People's Republic of China;* orcid.org/0000-0002-8835-4684

Jin-An Shi − *School of Physical Sciences, CAS Key Laboratory of Vacuum Physics, University of Chinese Academy of Sciences, Beijing 100049, People's Republic of China*

Xiangdong Guo − *CAS Key Laboratory of Nanophotonic Materials and Devices, CAS Key Laboratory of Standardization and Measurement for Nanotechnology, CAS Center for Excellence in Nanoscience, National Center for Nanoscience and Technology, Beijing 100190, People's Republic of China*

Yonggang Zuo − *The Key Laboratory of Unconventional Metallurgy, Ministry of Education, Faculty of Metallurgical and Energy Engineering, Kunming University of Science and Technology, Kunming 650093, People's Republic of China*

https://doi.org/10.1021/acs.nanolett.1c04598
Nano Lett. 2022, 22, 2725−2733

Ruijie Li − *School of Materials Science and Engineering, Peking University, Beijing 100871, People's Republic of China*

Hao Hong − *State Key Lab for Mesoscopic Physics and Frontiers Science Center for Nano-optoelectronics, Collaborative Innovation Center of Quantum Matter, School of Physics, Peking University, Beijing 100871, People's Republic of China*

Ning Li − *International Center for Quantum Materials, School of Physics and Electron Microscopy Laboratory, School of Physics, Peking University, Beijing 100871, People's Republic of China*

Kai Xu − *School of Physical Sciences, CAS Key Laboratory of Vacuum Physics, University of Chinese Academy of Sciences, Beijing 100049, People's Republic of China*

Xinyu Huang − *Advanced Research Institute of Multidisciplinary Science, Beijing Institute of Technology, Beijing 100081, People's Republic of China*

Huifeng Tian − *School of Materials Science and Engineering, Peking University, Beijing 100871, People's Republic of China*

Ying Yang − *Center for Quantum Transport and Thermal Energy Science, School of Physics and Technology, Nanjing Normal University, Nanjing 210023, People's Republic of China*

Zhixin Yao − *School of Materials Science and Engineering, Peking University, Beijing 100871, People's Republic of China; Key Laboratory of Interface Science and Engineering in Advanced Materials, Ministry of Education, Taiyuan University of Technology, Taiyuan 030024, People's Republic of China*

PeiChi Liao − *School of Materials Science and Engineering, Peking University, Beijing 100871, People's Republic of China*

Xiao Li − *Center for Quantum Transport and Thermal Energy Science, School of Physics and Technology, Nanjing Normal University, Nanjing 210023, People's Republic of China*

Junjie Guo − *Key Laboratory of Interface Science and Engineering in Advanced Materials, Ministry of Education, Taiyuan University of Technology, Taiyuan 030024, People's Republic of China;* orcid.org/0000-0002-3414-3734

Yuang Huang − *Advanced Research Institute of Multidisciplinary Science, Beijing Institute of Technology, Beijing 100081, People's Republic of China*

Peng Gao − *International Center for Quantum Materials, School of Physics, Electron Microscopy Laboratory, School of Physics, and Interdisciplinary Institute of Light-Element Quantum Materials and Research Center for Light-Element Advanced Materials, Peking University, Beijing 100871, People's Republic of China;* orcid.org/0000-0003-0860-5525

Lifen Wang − *Beijing National Laboratory for Condensed Matter Physics, Institute of Physics, Chinese Academy of Sciences, Beijing 100190, People's Republic of China; Songshan Lake Materials Laboratory, Dongguan 523808, People's Republic of China;* orcid.org/0000-0002-8468-5048

Xiaoxia Yang − *CAS Key Laboratory of Nanophotonic Materials and Devices, CAS Key Laboratory of Standardization and Measurement for Nanotechnology, CAS Center for Excellence in Nanoscience, National Center for Nanoscience and Technology, Beijing 100190, People's Republic of China*

Qing Dai − *CAS Key Laboratory of Nanophotonic Materials and Devices, CAS Key Laboratory of Standardization and Measurement for Nanotechnology, CAS Center for Excellence in Nanoscience, National Center for Nanoscience and Technology, Beijing 100190, People's Republic of China;* orcid.org/0000-0002-1750-0867

EnGe Wang − *International Center for Quantum Materials, School of Physics and Interdisciplinary Institute of Light-Element Quantum Materials and Research Center for Light-Element Advanced Materials, Peking University, Beijing 100871, People's Republic of China; Songshan Lake Materials Laboratory, Dongguan 523808, People's Republic of China; School of Physics, Liaoning University, Shenyang 110036, People's Republic of China*

Kaihui Liu − *State Key Lab for Mesoscopic Physics and Frontiers Science Center for Nano-optoelectronics, Collaborative Innovation Center of Quantum Matter, School of Physics and Interdisciplinary Institute of Light-Element Quantum Materials and Research Center for Light-Element Advanced Materials, Peking University, Beijing 100871, People's Republic of China;* orcid.org/0000-0002-8781-2495

Wu Zhou − *School of Physical Sciences, CAS Key Laboratory of Vacuum Physics, University of Chinese Academy of Sciences, Beijing 100049, People's Republic of China; CAS Center for Excellence in Topological Quantum Computation, University of Chinese Academy of Sciences, Beijing 100049, People's Republic of China*

Xiaohui Yu − *Beijing National Laboratory for Condensed Matter Physics, Institute of Physics, Chinese Academy of Sciences, Beijing 100190, People's Republic of China; Songshan Lake Materials Laboratory, Dongguan 523808, People's Republic of China;* orcid.org/0000-0001-8880-2304

Liangbo Liang − *Center for Nanophase Materials Sciences, Oak Ridge National Laboratory, Oak Ridge, Tennessee 37831, United States;* orcid.org/0000-0003-1199-0049

Ying Jiang − *International Center for Quantum Materials, School of Physics and Interdisciplinary Institute of Light-Element Quantum Materials and Research Center for Light-Element Advanced Materials, Peking University, Beijing 100871, People's Republic of China*

Complete contact information is available at: https://pubs.acs.org/10.1021/acs.nanolett.1c04598

Author Contributions

[◊]Y.L. and X.Z. contributed equally to this work.

Author Contributions

L.L. and X.-Z.L.conceived the project. Y.L., J.W., R.L., Y.Z., and K.L. prepared samples. X.Z., L.L., X.-Z.L. Y.Y., X.L., and E.W. performed the DFT calculations. N.L., Z.Y., J.G., L.W., and P.G. performed the electron microscope measurements on isotopically engineered BN flakes. K.X., J.-A.S. and W.Z. performed the STEM characterizations on heterostructures. X.G., X.Y., and Q.D. performed the FTIR measurements. Y.L., H.H., X.H., H.T., P.L., and Y.H. performed the Raman and PL measurements. Y.L., X.M., and X.Y. performed high pressure measurements. Y.L., X.Z., Y.J., L.L., X.-Z.L.and L.L. analyzed data and e the manuscript, and all authors discussed and commented on it.

Notes

The authors declare no competing financial interest.

https://doi.org/10.1021/acs.nanolett.1c04598
Nano Lett. 2022, 22, 2725−2733

■ ACKNOWLEDGMENTS

This work was supported by the National Natural Science Foundation of China (Project Nos. U1932153, 11974001, 11934003, 52025023, 51991342, 11888101, 52125307, 52021006), the National Key R&D Program of China (2019YFA0307800, 2021YFA1400500), the Beijing Natural Science Foundation (Z190011), the Key Research Program of Frontier Sciences, CAS (QYZDB-SSW-JSC019), and the Strategic Priority Research Program of the Chinese Academy of Sciences (Grant No. XDB28000000). We acknowledge the Electron Microscopy Laboratory at Peking University for the use of an electron microscope. L.L. acknowledges work at the Center for Nanophase Materials Sciences, which is a U.S. Department of Energy Office of Science User Facility.

■ REFERENCES

(1) Novoselov, K. S.; Mishchenko, A.; Carvalho, A.; Neto, A. H. C. 2D materials and van der Waals heterostructures. *Science* **2016**, *353*, 6298.

(2) Jariwala, D.; Marks, T. J.; Hersam, M. C. Mixed-dimensional van der Waals heterostructures. *Nat. Mater.* **2017**, *16* (2), 170−181.

(3) Gorbachev, R. V.; Geim, A. K.; Katsnelson, M. I.; Novoselov, K. S.; Tudorovskiy, T.; Grigorieva, I. V.; MacDonald, A. H.; Morozov, S. V.; Watanabe, K.; Taniguchi, T.; Ponomarenko, L. A. Strong Coulomb drag and broken symmetry in double-layer graphene. *Nat. Phys.* **2012**, *8* (12), 896−901.

(4) Fang, H.; Battaglia, C.; Carraro, C.; Nemsak, S.; Ozdol, B.; Kang, J. S.; Bechtel, H. A.; Desai, S. B.; Kronast, F.; Unal, A. A.; Conti, G.; Conlon, C.; Palsson, G. K.; Martin, M. C.; Minor, A. M.; Fadley, C. S.; Yablonovitch, E.; Maboudian, R.; Javey, A. Strong interlayer coupling in van der Waals heterostructures built from single-layer chalcogenides. *Proc. Natl. Acad. Sci. U.S.A.* **2014**, *111* (17), 6198−6202.

(5) Jin, C. H.; Kim, J.; Suh, J.; Shi, Z. W.; Chen, B.; Fan, X.; Kam, M.; Watanabe, K.; Taniguchi, T.; Tongay, S.; Zettl, A.; Wu, J. Q.; Wang, F. Interlayer electron-phonon coupling in WSe_2/BN heterostructures. *Nat. Phys.* **2017**, *13* (2), 127−131.

(6) Lin, M. L.; Zhou, Y.; Wu, J. B.; Cong, X.; Liu, X. L.; Zhang, J.; Li, H.; Yao, W.; Tan, P. H. Cross-dimensional electron-phonon coupling in van der Waals heterostructures. *Nat. Commun.* **2019**, *10*, 2419.

(7) Chen, C.; Chen, X. L.; Yu, H. Y.; Shao, Y. C.; Guo, Q. S.; Deng, B. C.; Lee, S.; Ma, C.; Watanabe, K.; Taniguchi, T.; Park, J. G.; Huang, S. X.; Yao, W.; Xia, F. N. Symmetry-Controlled Electron-Phonon Interactions in van der Waals Heterostructures. *ACS Nano* **2019**, *13* (1), 552−559.

(8) Chow, C. M.; Yu, H. Y.; Jones, A. M.; Yan, J. Q.; Mandrus, D. G.; Taniguchi, T.; Watanabe, K.; Yao, W.; Xu, X. D. Unusual Exciton-Phonon Interactions at van der Waals Engineered Interfaces. *Nano Lett.* **2017**, *17* (2), 1194−1199.

(9) Giustino, F. Electron-phonon interactions from first principles. *Rev. Mod. Phys.* **2017**, *89* (1), 015003.

(10) Du, L. J.; Zhao, Y. C.; Jia, Z. Y.; Liao, M. Z.; Wang, Q. Q.; Guo, X. D.; Shi, Z. W.; Yang, R.; Watanabe, K.; Taniguchi, T.; Xiang, J. Y.; Shi, D. X.; Dai, Q.; Sun, Z. P.; Zhang, G. Y. Strong and tunable interlayer coupling of infrared-active phonons to excitons in van der Waals heterostructures. *Phys. Rev. B* **2019**, *99* (20), 205410.

(11) Meng, Y. Z.; Wang, T. M.; Li, Z. P.; Qin, Y.; Lian, Z.; Chen, Y. W.; Lucking, M. C.; Beach, K.; Taniguchi, T.; Watanabe, K.; Tongay, S.; Song, F. Q.; Terrones, H.; Shi, S. F. Excitonic Complexes and Emerging Interlayer Electron-Phonon Coupling in BN Encapsulated Monolayer Semiconductor Alloy: $WS_{0.6}Se_{1.4}$. *Nano Lett.* **2019**, *19* (1), 299−307.

(12) Li, Y. F.; Wen, X.; Tan, C. J.; Li, N.; Li, R. J.; Huang, X. Y.; Tian, H. F.; Yao, Z. X.; Liao, P. C.; Yu, S. L.; Liu, S. Z.; Li, Z. J.; Guo, J. J.; Huang, Y.; Gao, P.; Wang, L. F.; Bai, S. L.; Liu, L. Synthesis of centimeter-scale high-quality polycrystalline hexagonal boron nitride films from Fe fluxes. *Nanoscale* **2021**, *13* (25), 11223−11231.

(13) Vuong, T. Q. P.; Liu, S.; Van der Lee, A.; Cusco, R.; Artus, L.; Michel, T.; Valvin, P.; Edgar, J. H.; Cassabois, G.; Gil, B. Isotope engineering of van der Waals interactions in hexagonal boron nitride. *Nat. Mater.* **2018**, *17* (2), 152−158.

(14) Giles, A. J.; Dai, S. Y.; Vurgaftman, I.; Man, T. H.; Liu, S.; Lindsay, L.; Ellis, C. T.; Assefa, N.; Chatzakis, I.; Reinecke, T. L.; Tischler, J. G.; Fogler, M. M.; Edgar, J. H.; Basov, D. N.; Caldwell, J. D. Ultralow-loss polaritons in isotopically pure boron nitride. *Nat. Mater.* **2018**, *17* (2), 134−139.

(15) Cusco, R.; Artus, L.; Edgar, J. H.; Liu, S.; Cassabois, G.; Gil, B. Isotopic effects on phonon anharmonicity in layered van der Waals crystals: Isotopically pure hexagonal boron nitride. *Phys. Rev. B* **2018**, *97* (15), 155435.

(16) Cusco, R.; Edgar, J. H.; Liu, S.; Li, J. H.; Artus, L. Isotopic Disorder: The Prevailing Mechanism in Limiting the Phonon Lifetime in Hexagonal BN. *Phys. Rev. Lett.* **2020**, *124* (16), 167402.

(17) Cusco, R.; Edgar, J. H.; Liu, S.; Cassabois, G.; Gil, B.; Artus, L. Influence of isotopic substitution on the anharmonicity of the interlayer shear mode of h-BN. *Phys. Rev. B* **2019**, *99* (8), 085428.

(18) Zhang, J.; Wang, J. H.; Chen, P.; Sun, Y.; Wu, S.; Jia, Z. Y.; Lu, X. B.; Yu, H.; Chen, W.; Zhu, J. Q.; Xie, G. B.; Yang, R.; Shi, D. X.; Xu, X. L.; Xiang, J. Y.; Liu, K. H.; Zhang, G. Y. Observation of Strong Interlayer Coupling in MoS_2/WS_2 Heterostructures. *Adv. Mater.* **2016**, *28* (10), 1950−1956.

(19) Carvalho, B. R.; Malard, L. M.; Alves, J. M.; Fantini, C.; Pimenta, M. A. Symmetry-Dependent Exciton-Phonon Coupling in 2D and Bulk MoS_2 Observed by Resonance Raman Scattering. *Phys. Rev. Lett.* **2015**, *114* (13), 136403.

(20) Widulle, F.; Ruf, T.; Buresch, O.; Debernardi, A.; Cardona, M. Raman study of isotope effects and phonon eigenvectors in SiC. *Phys. Rev. Lett.* **1999**, *82* (15), 3089−3092.

(21) Mascarenhas, A.; Katayamayoshida, H.; Pankove, J.; Deb, S. K. Copper Isotope Effect in Raman-Scattering on Superconducting $YBa_2Cu_3O_{7-X}$. *Phys. Rev. B* **1989**, *39* (7), 4699−4700.

(22) Li, X. F.; Zhang, J. J.; Puretzky, A. A.; Yoshimura, A.; Sang, X. H.; Cui, Q. N.; Li, Y. Y.; Liang, L. B.; Ghosh, A. W.; Zhao, H.; Unocic, R. R.; Meunier, V.; Rouleau, C. M.; Sumpter, B. G.; Geohegan, D. B.; Xiao, K. Isotope-Engineering the Thermal Conductivity of Two-Dimensional MoS_2. *ACS Nano* **2019**, *13* (2), 2481−2489.

(23) Wu, W.; Morales-Acosta, M. D.; Wang, Y. Q.; Pettes, M. T. Isotope Effect in Bilayer WSe_2. *Nano Lett.* **2019**, *19* (3), 1527−1533.

(24) Cusco, R.; Gil, B.; Cassabois, G.; Artus, L. Temperature dependence of Raman-active phonons and anharmonic interactions in layered hexagonal BN. *Phys. Rev. B* **2016**, *94* (15), 155435.

(25) Zhu, B. R.; Chen, X.; Cui, X. D. Exciton Binding Energy of Monolayer WS_2. *Sci. Rep.* **2015**, *5*, 9218.

(26) Park, H.; Shin, G. H.; Lee, K. J.; Choi, S. Y. Probing temperature-dependent interlayer coupling in a MoS_2/h-BN heterostructure. *Nano Research* **2020**, *13* (2), 576−582.

(27) Tongay, S.; Zhou, J.; Ataca, C.; Lo, K.; Matthews, T. S.; Li, J. B.; Grossman, J. C.; Wu, J. Q. Thermally Driven Crossover from Indirect toward Direct Bandgap in 2D Semiconductors: $MoSe_2$ versus MoS_2. *Nano Lett.* **2012**, *12* (11), 5576−5580.

(28) Wang, F.; Wang, J. Y.; Guo, S.; Zhang, J. Z.; Hu, Z. G.; Chu, J. H. Tuning Coupling Behavior of Stacked Heterostructures Based on MoS_2, WS_2, and WSe_2. *Sci. Rep.* **2017**, *7*, 44712.

(29) Pease, R. S. An X-Ray Study of Boron Nitride. *Acta Crystallogr.* **1952**, *5* (3), 356−361.

(30) Yankowitz, M.; Jung, J.; Laksono, E.; Leconte, N.; Chittari, B. L.; Watanabe, K.; Taniguchi, T.; Adam, S.; Graf, D.; Dean, C. R. Dynamic band-structure tuning of graphene moire superlattices with pressure. *Nature* **2018**, *557* (7705), 404−408.

(31) Nayak, A. P.; Bhattacharyya, S.; Zhu, J.; Liu, J.; Wu, X.; Pandey, T.; Jin, C. Q.; Singh, A. K.; Akinwande, D.; Lin, J. F. Pressure-induced semiconducting to metallic transition in multilayered molybdenum disulphide. *Nat. Commun.* **2014**, *5*, 3731.

(32) Fu, L.; Wan, Y.; Tang, N.; Ding, Y. M.; Gao, J.; Yu, J. C.; Guan, H. M.; Zhang, K.; Wang, W. Y.; Zhang, C. F.; Shi, J. J.; Wu, X.; Shi, S.

https://doi.org/10.1021/acs.nanolett.1c04598
Nano Lett. 2022, 22, 2725−2733

F.; Ge, W. K.; Dai, L.; Shen, B. K-Λ crossover transition in the conduction band of monolayer MoS_2 under hydrostatic pressure. *Sci. Adv.* **2017**, *3* (11), 1700162.
(33) Ma, X. L.; Fu, S. H.; Ding, J. W.; Liu, M.; Bian, A.; Hong, F.; Sun, J. T.; Zhang, X. X.; Yu, X. H.; He, D. W. Robust Interlayer Exciton in $WS_2/MoSe_2$ van der Waals Heterostructure under High Pressure. *Nano Lett.* **2021**, *21* (19), 8035−8042.
(34) Wang, L.; Meric, I.; Huang, P. Y.; Gao, Q.; Gao, Y.; Tran, H.; Taniguchi, T.; Watanabe, K.; Campos, L. M.; Muller, D. A.; Guo, J.; Kim, P.; Hone, J.; Shepard, K. L.; Dean, C. R. One-Dimensional Electrical Contact to a Two-Dimensional Material. *Science* **2013**, *342* (6185), 614−617.
(35) Nayak, A. P.; Yuan, Z.; Cao, B.; Liu, J.; Wu, J.; Moran, S. T.; Li, T.; Akinwande, D.; Jin, C.; Lin, J.-F. Pressure-Modulated Conductivity, Carrier Density, and Mobility of Multilayered Tungsten Disulfide. *ACS Nano* **2015**, *9* (9), 9117−9123.
(36) Han, B.; Li, F. F.; Li, L.; Huang, X. L.; Gong, Y. B.; Fu, X. P.; Gao, H. X.; Zhou, Q.; Cui, T. Correlatively Dependent Lattice and Electronic Structural Evolutions in Compressed Monolayer Tungsten Disulfide. *J. Phys. Chem. Lett.* **2017**, *8* (5), 941−947.
(37) Duwal, S.; Yoo, C. S. Shear-Induced Isostructural Phase Transition and Metallization of Layered Tungsten Disulfide under Nonhydrostatic Compression. *J. Phys. Chem. Lett.* **2016**, *120* (9), 5101−5107.
(38) Li, R.; Li, Y.; Yang, Y.; Huang, X.; Zhang, S.; Tian, H.; Huang, X.; Yao, Z.; Liao, P.; Yu, S.; Liu, S.; Li, Z.; Huang, Y.; Guo, J.; Mei, F.; Wang, L.; Li, X.; Liu, L. Isotope Effect of Hydrogen Functionalization in Layered Germanane: Implications for Germanane-Based Optoelectronics. *ACS Appl. Nano Mater.* **2021**, *4* (12), 13708−13715.

https://doi.org/10.1021/acs.nanolett.1c04598
Nano Lett. 2022, 22, 2725−2733